Classification of Persistent Heavy Rainfall Events over South China and Associated Moisture Source Analysis

LIU Ruixin[1,2] (刘瑞鑫), SUN Jianhua[1,2*] (孙建华), WEI Jie[1] (卫 捷), and FU Shenming[1] (傅慎明)

1 *Key Laboratory of Cloud-Precipitation Physics and Severe Storms (LACS), Institute of Atmospheric Physics, Chinese Academy of Sciences, Beijing* 100029

2 *University of Chinese Academy of Sciences, Beijing* 100049

(Received February 29, 2016; in final form July 18, 2016)

ABSTRACT

Persistent heavy rainfall events (PHREs) over South China during 1981–2014 were selected and classified by an objective method, based on the daily precipitation data at 752 stations in China. The circulation characteristics, as well as the dry-cold air and moisture sources of each type of PHREs were examined. The main results are as follows. A total of 32 non-typhoon influenced PHREs in South China were identified over the study period. By correlation analysis, the PHREs are divided into three types: SC-A type, with its main rainbelt located in the coastal areas and the northeast of Guangdong Province; SC-B type, with its main rainbelt between Guangdong Province and Guangxi Region; and SC-C type, with its main rainbelt located in the north of Guangxi Region. For the SC-A events, dry-cold air flew to South China under the steering effect of troughs in the middle troposphere which originated from the Ural Mountains and West Siberia Plain; whereas, the SC-C events were not influenced by the cold air from high latitudes. There were three water vapor pathways from low-latitude areas for both the SC-A and SC-C PHREs. The tropical Indian Ocean was the main water vapor source for these two PHRE types, while the South China Sea also contributed to the SC-C PHREs. In addition, the SC-A events were also influenced by moist and cold air originating from the Yellow Sea. Generally, the SC-C PHREs belonged to a warm-sector rainfall type, whose precipitation areas were dominated by southwesterly wind, and the convergence in wind speed was the main reason for precipitation.

Key words: persistent heavy rainfall events, South China, warm-sector rainfall, dry-cold air, moisture source, water vapor transport

Citation: Liu Ruixin, Sun Jianhua, Wei Jie, et al., 2016: Classification of persistent heavy rainfall events over South China and associated moisture source analysis. *J. Meteor. Res.*, **30**(5), 678–693, doi: 10.1007/s13351-016-6042-x.

1. Introduction

Under the influences of the East Asian summer monsoon and the complex East Asian terrain (Tao, 1980), China is one of the regions with most abundant rain. In particular, China experiences numerous rainfall events that feature large amounts of precipitation and long durations, which together represent extremely severe and often deadly meteorological disasters. Every year, flash floods, urban waterlogging or landslides, triggered by persistent heavy rainfall events (PHREs), pose serious threat to the safety of people and cause substantial economic loss. For instance, PHREs in 1998 and 1999 triggered severe flooding events in the Yangtze River valley (Tao et al., 2001, 2004; Zhao et al., 2004), and a catastrophic flood due to PHREs occurred over South China in 1994 (Shi and Ding, 2000; Sun and Zhao, 2002a, b). Owing to the great importance of PHREs, revealing their main mechanisms of evolution and predicting their activities (occurrence, duration, intensity, etc.) have become a highly important topic of research (Yu and Li, 2012). In an early study, Tao (1980) classified the large-scale circulations favorable for PHREs into the meridional

Supported by the National (Key) Basic Research and Development (973) Program of China (2012CB417201) and National Natural Science Foundation of China (41375053).

*Corresponding author: sjh@mail.iap.ac.cn.

type and zonal type. He pointed out that when a PHRE occurs, the planetary-scale circulation maintains a favorable pattern or experiences a rapid adjustment. Abundant water vapor transport, stable maintenance of synoptic-scale systems, and favorable terrain-related effects may sustain a PHRE for more than a few days. Bao (2007) discussed the characteristics and variations of PHREs in the last 50 years over China and summarized four kinds of PHREs: the Bohai Sea–western Liaoning Province type; the northern meridional type; the southern front type; and the tropical depression type. Chen and Zhai (2014) classified PHREs in eastern–central China into a double-blocking high pattern and a single-blocking high pattern. Moreover, Sun and Ding (2002) pointed out that the monsoons transport large quantities of warm-moist air to precipitation areas, providing abundant moisture and unstable energy conditions for rainfall events.

South China, influenced by the East Asian summer monsoon, Indian monsoon, western Pacific subtropical high (WPSH), and the dynamic/thermodynamic effects of the Tibetan Plateau, is an important rainy region (Tao, 1980; Zhao et al., 2004; Zhou et al., 2008). In recent years, the frequency of heavy rainfall events in South China has increased significantly (Fu et al., 2016; Li et al., 2016), and serious floods have occurred due to such torrential rainfalls (e.g., the devastating floods in 1994, 1998, 2005, and 2008). A number of studies have been conducted to classify PHREs over South China (Hu et al., 2013), and some have also focused on the underlying mechanisms (Huang et al., 2005; Ren et al., 2006; Feng et al., 2011; Chen et al., 2012a; Li and Leung, 2013). For example, Hu et al. (2013) classified the pre-rainy season rainfall events in South China into the southeast coast type, the northern type, and the southwest coast type. Furthermore, the causes of rainfall over South China may be related to tropical cyclone activities (Ren et al., 2006; Chen et al., 2012a) and midlatitude westerly troughs or the intertropical convergence zone (Huang et al., 2005).

Wang et al. (2014) selected PHREs over southern China using three criteria; firstly, PHREs had to cover more than 10 data grids in the study area; secondly, daily precipitation exceeded 50 mm and lasted for at least five days; and finally, for two continuous days of rainfall, the degree of overlapping of the rain band was greater than 20%. Given that PHREs occur at different times and in different regions, we first need to deal with their classification. Thus far, most PHRE classifications for South China are mainly based on the circulation features of associated weather. However, this suffers from subjectivity, especially when faced with large amounts of data. Therefore, the primary purpose of the present study is to classify PHREs over South China by using an objective method that considers both the precipitation areas and critical weather systems. On this basis, we could then analyze the characteristics of PHREs over South China from type to type.

Persistent precipitation is generally influenced by both moist-warm air and dry-cold air activities. Moreover, warm-sector rainfall is common in South China, so sufficient moisture is an important condition for the maintenance of PHREs. Ding (1992) proposed that water vapor in South China mainly comes from the Bay of Bengal and the South China Sea. Tian et al. (2004) pointed out that climatologically, three main monsoonal flows transport water vapor to China during boreal summer at low latitudes. One of these flows is the southwesterly flow associated with the Indian summer monsoon, and the other two are the southerly flow and southeasterly flow related to the South China Sea monsoon and the subtropical monsoon, respectively (Zhou and Yu, 2005; Chow et al., 2008). Among these flows, the southwesterly flow and southerly flow have an influence on PHREs over South China. We come to realize that these discussions about water vapor transport are primarily based on climate timescales, without focusing on specific cases. Such studies are unable to analyze the contribution of different water vapor pathways. There are two widely used models for tracking air parcels: FLEXPART (the Flexible Particle Dispersion Model) (Qing et al., 2014) and HYSPLIT (the Hybrid Single Particle Lagrangian Integrated Trajectory Model). In this study, HYSPLIT is used to analyze the sources and pathways of water vapor and dry-cold air. Previously, the model has been utilized to analyze the

transport and contribution of water vapor in various weather processes (Jiang et al., 2011; Fuhrmann and Konrad II, 2013; Sun et al., 2016).

Previous studies have shown that some rainfall events over South China apparently feature no cold air. Huang (1986) proposed the concept of warm-sector rainfall and defined it as rainfall that takes place inside the warm-sector, 200–300 km from the ground surface front, or occurs in the southwesterly and southeasterly convergent airflow, or happens in the southwesterly airflow without horizontal wind shear. Here, the warm-sector rainfall does not include any rainfall event that is affected by typhoons or other tropical systems. Additionally, Chen et al. (2012b) divided warm-sector rainfall in South China into three types related to shear lines, low vortexes, and southerly wind velocity shear.

To continue the study of PHREs over South China, and following Wang et al. (2014), we adopted objective standards to select PHREs in the region 18°–26°N, 105°–120°E (purple rectangle in Fig. 1) during the warm seasons (April–November) of 1981–2014. Composite analysis of the selected PHREs is done to identify the similarities and differences in multiscale circulations of these events. Additionally, HYSPLIT is used to analyze the sources of water vapor and dry-cold air for different types of PHREs over South China. Following this introduction, Section 2 introduces the data and methodology used to select and classify the PHREs; Section 3 analyzes the composite circulation characteristics associated with the selected PHREs; the sources and transport of water vapor and cold air for different types of PHRE are investigated in Section 4, based on the HYSPLIT results; Section 5 describes the key characteristics of the warm-sector rainfall; and finally, Section 6 discusses and summarizes the main findings.

2. Data and methodology

Daily precipitation observational data at 752 stations from the China Meteorological Administration during the period 1981–2014 were used to identify PHREs over South China. Because the stations were unevenly distributed and the corresponding precipitation featured large regional differences, the station data were interpolated to a 0.25° × 0.25° grid following the Cressman interpolation method as used by Wang et al. (2014). The PHREs were then analyzed by using the interpolated precipitation data. Moreover, selection of the PHREs also considered the annual typhoon track data from the China Meteorological Administration Joint Typhoon Warning Center, to eliminate those specific PHREs influenced by typhoons and tropical depressions. The daily NCEP–NCAR reanalysis data were also used. The outgoing longwave radiation (OLR) satellite data were from the NOAA. The reanalysis data, on a horizontal resolution of 2.5° × 2.5°, were used to analyze the weather circulation during the period of the PHREs. Furthermore, 6-h ECMWF Interim Reanalysis data, at a horizontal resolution of 0.75° × 0.75° and 24 vertical layers (Simmons et al., 2007), were utilized for analyzing the warm-sector rainfall.

Version 4.9 of HYSPLIT, which adopts the Lagrangian method to calculate advection and diffusion, was used to analyze the sources and pathways of water vapor. The model is typically used for tracking the trajectory of particles carried by airflow. During the model integration, the data were interpolated to a terrain-following coordinate (Draxler and Hess, 1998). The simulation domain was specified as the land area covering 20.0°–27.5°N, 105°–120°E, and three height levels of 500, 1500, and 3000 m were used to initiate the simulation. There were 57 initial trajectory points in the entire simulation. To obtain the location of the track points and the corresponding physical quantities on an hourly basis, 10-day duration trajectory tracking for every PHRE was simulated on the basis of these 57 points. Since the number of simulated output trajectories was too large, we analyzed the contribution of different moisture pathways according to the closest trajectory path cluster principle to identify the more significant trajectory distribution. The water vapor pathway contribution rate was calculated as follows (Sun et al., 2016):

$$Q_{\text{all}} = \left(\sum_{1}^{m} \sum_{t=1}^{240} q_t \Big/ \sum_{1}^{n} \sum_{t=1}^{240} q_t \right) \times 100\%, \qquad (1)$$

where q_t is the air mass specific humidity of each simu-

lation time, m is the number of each cluster containing tracks, and n is the number of all tracks.

The focus of this study was 32 selected PHREs over South China, which were not influenced by typhoons during 1981–2014. The longest PHRE persisted for 13 days from 1 to 13 June 2001. Meanwhile, 19 of the PHREs occurred during April–June and 13 during July–October, with the most PHREs appearing from June to July and the largest number of cases in June, which was consistent with the findings of Xie et al. (2006). Although the selection process emphasized that the duration of PHREs could not be shorter than 5 days, the PHREs' durations differed, which would have influenced the amount of precipitation accumulated for each case. Therefore, this study was based on an objective method, which analyzed the normalized anomaly of each case's average daily precipitation. That is, $N = (X - \mu)/\sigma$, where X is a grid of a physical quantity (average daily precipitation), μ is the 30-yr climatological average grid of the physical quantity during 1981–2010, and σ is the standard deviation. Meanwhile, the average daily precipitation normalized anomaly correlation coefficient between any two PHREs was also calculated, following the method introduced by Santer et al. (1993). According to the correlation coefficients among the PHREs (with correlation coefficients above 0.3 as the same type) and the precipitation central areas, an initial classification of the PHREs over South China was conducted. Accordingly, the selected PHREs were classified when the following criteria were satisfied: (1) the northern part of the study area (30°–50°N) and west of 120°E featured a low trough; and (2) the precipitation area featured a front or any other major system that influenced precipitation.

The details of the classification are shown in Table 1 and Fig. 2. According to the spatial distribution of the rainbelt, PHREs over South China were divided

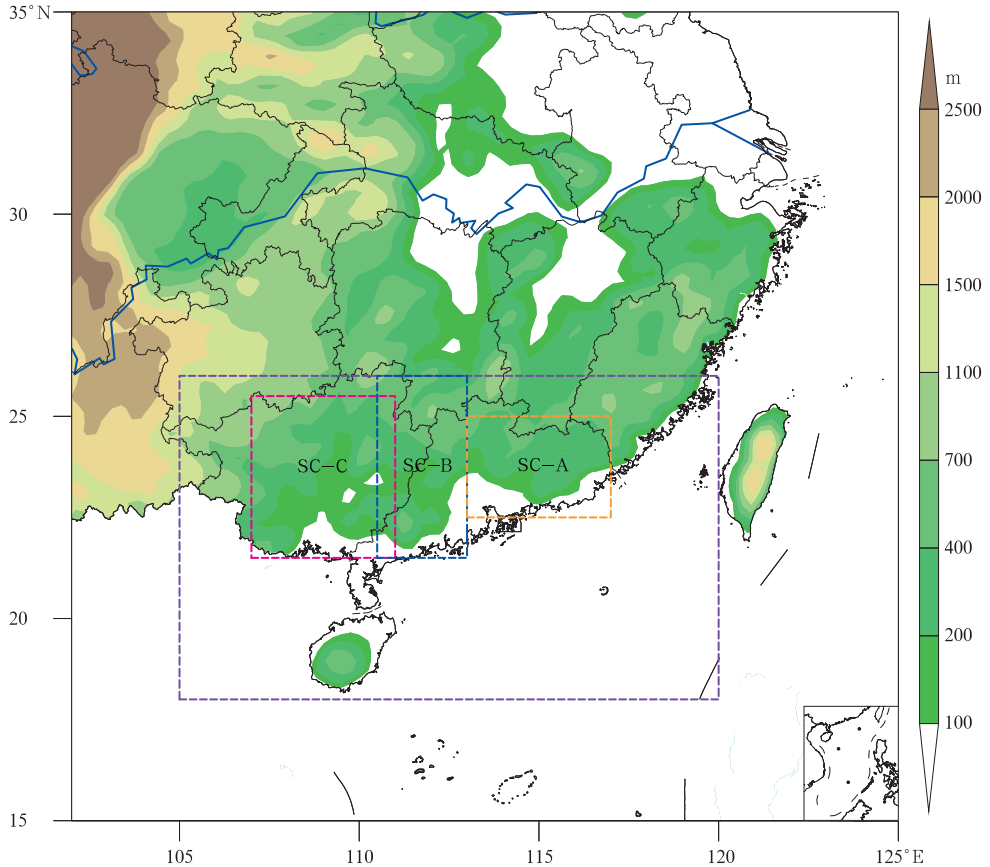

Fig. 1. The study domain and topography (shaded; m). South China is outlined by a purple rectangle. The orange, blue, and pink rectangles represent the regions of the SC-A, SC-B, and SC-C type PHREs, respectively. See Table 1 for details on the different PHRE types.

Table 1. Classification of the selected PHREs over South China

Type	Occurrence time	Trough at 30°–50°N and west of 120°E at 500 hPa	A front at 850 hPa above precipitation area	Main low-latitude system at 850 hPa
SC-A	2–6 July 1982	Yes	No	Wind shear
	13–18 May 1984	Yes	Yes	Wind shear
	29 May to 2 June 1989	Yes	Yes	Wind shear
	4–8 July 1992	Yes	Yes	Wind shear
	7–13 June 1993	No	No	Wind shear
	16–20 July 2002	Yes	No	Southwesterly ahead of vortex
	19–24 June 2005	Yes	Yes	Wind shear
	14–18 June 2010	Yes	Yes	Wind shear
SC-B	17–25 July 1994	Yes	No	Southwesterly ahead of vortex
	21–26 June 1996	Yes	Yes	Wind shear
	1–13 June 2001	Yes	Yes	Wind shear
	29 June to 3 July 2002	Yes	No	Southwesterly ahead of vortex
	15–19 June 2008	Yes	Yes	Wind shear
SC-C	27 August to 1 September 1988	No	No	Southwesterly ahead of vortex
	8–12 June 1991	Yes	No	Southwesterly ahead of trough
	4–9 July 1993	Yes	No	Southwesterly ahead of trough
	12–17 June 1994	No	No	Wind shear
	16–26 June 1998	No	No	Wind shear
	18–22 July 2004	No	No	Southwesterly ahead of trough
	1–8 June 2005	No	No	Southwesterly ahead of vortex

Note: these PHREs were not affected by typhoons.

into three types: SC-A type events, in which the main rainbelt was located in the coastal areas and northeast of Guangdong Province (eight cases); SC-B type events, in which the main rainbelt was between Guangdong Province and Guangxi Region (five cases); and SC-C type events, in which the main rainbelt was located in the north of Guangxi Region (seven cases). The selected PHREs included four cases identified by Bao (2007) that lasted more than 5 days from 1981 to 2005. Statistical analysis of meteorological variables (geopotential height, wind u and v) was carried out and these variables of the SC-B type events did not pass the significance test. Moreover, examination of the circulation during SC-B type events on an individual basis revealed that these cases differed notably; a common characteristic was not found. Therefore, we only focused on the circulation features of SC-A and SC-C PHREs, and their moisture sources. In addition, the warm-sector rainfall characteristics of the SC-C type events were also examined.

3. Composite circulation characteristics of the SC-A and SC-C PHREs

Based on the systems of influence (Table 1), a composite analysis of the SC-A and SC-C PHREs that occurred in South China was performed to identify the similarities and differences in their circulation characteristics and climatic mean circulation patterns (Figs. 3 and 4). As can be seen, for the SC-A events at 200 hPa (Fig. 3a), there was a deep trough between the east of Siberia and the Sea of Okhotsk at high latitude, while other parts of Eurasia basically had straight airflow. Moreover, the airflow was relatively straight from the west of Europe to Lake Baikal at mid latitudes. A deep trough whose southern tip reached south of 30°N existed near the Yangtze–Huaihe River basin and Japan Sea (negative geopotential height anomaly reaching the 90% confidence level). Meanwhile, the zonal coverage of the jet stream was larger than that of the climate mean and the location was farther south, which was conducive to driving cold air to the precipitation area.

The composite circulation characteristics at 500 hPa (Fig. 3b) were similar to those at 200 hPa. The midlatitude trough in the east of China was favorable to the transport of cold air to South China. During the SC-A events, the west of the WPSH occupied the South China Sea, and it stretched farther west and so-

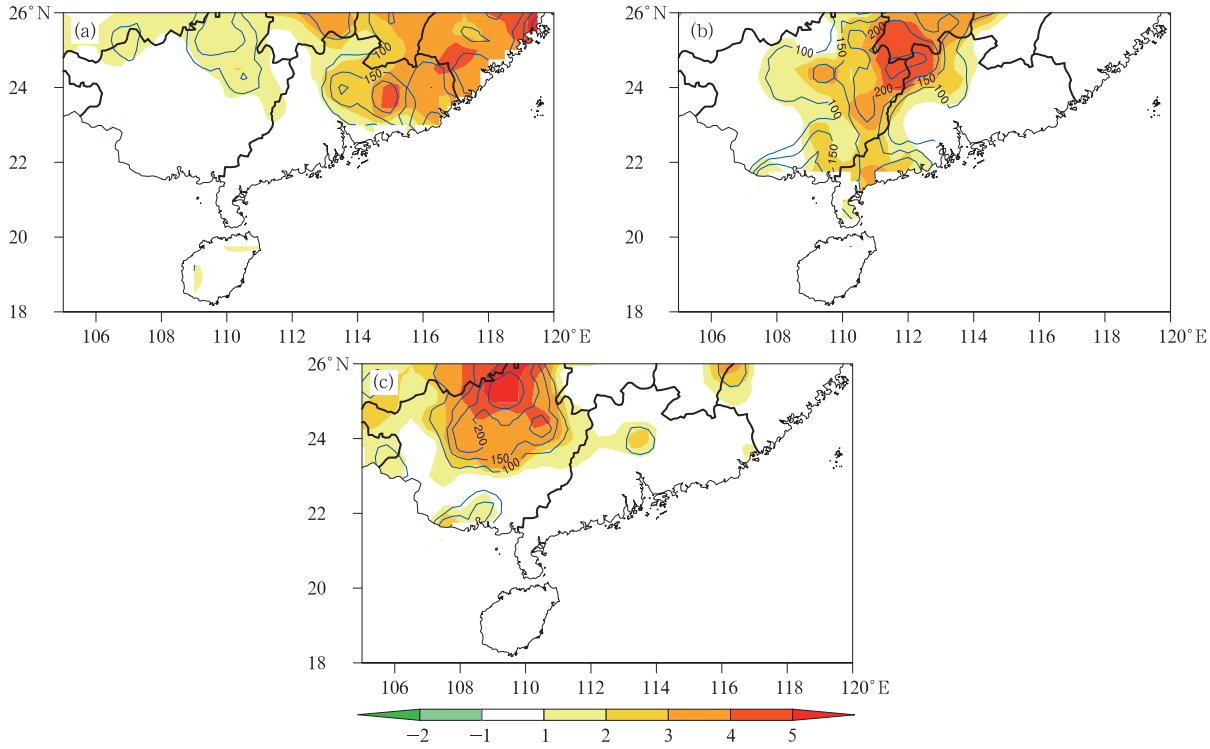

Fig. 2. Normalized mean daily precipitation anomalies (color shading; mm) and accumulated precipitation (contours; mm) of the PHREs. (a) SC-A; (b) SC-B; and (c) SC-C.

uth than the climatology, with stronger intensity. Additionally, the convection over the northwestern edge of the WPSH was particularly active, and the OLR negative anomaly center reached –1.5 or more near Guangdong and the coasts of Fujian (Fig. 3b).

The WPSH was stronger and covered a broad region at 850 hPa (Fig. 3c), continually providing abundant moisture from the west of the WPSH for the occurrence of PHREs. From the cross-section along the precipitation center, it can be seen that the lower layer above the precipitation area was unstable while the middle levels featured neutral stratification. As a result, upward motion controlled the entire troposphere, which was conducive to the maintenance of precipitation (Fig. 3d).

As for the composite circulation of the SC-C type events, the characteristics were largely the same at 200 and 500 hPa. During these events, a trough developed in the east of the North Atlantic Ocean at high latitude and another shallow trough near Lake Baikal. A broad ridge that reached the 90% confidence level existed between the two troughs near the Ural Mountains, presenting a "– + –" geopotential height anomaly distribution. Straight airflow controlled the midlatitude area, while a shallow trough existed near the Yangtze–Huaihe River basin. Besides, around the Asia–Pacific region, the upper-level jet steam was significantly weaker than the climate mean (Fig. 4a), such that the weak activities of the planetary-scale and synoptic-scale systems made the cold air inactive in the lower and middle troposphere. The weak intensity of the upper-level jet stream for the SC-C type events was one of the most significant differences found between the two types of PHREs. The west of South China was under the control of the eastern section of the 12520-gpm isohypse (Fig. 4a). Guangxi Region was dominated by the eastern section of the South Asia high, and correspondingly its associated upper-level divergent region was over South China. Therefore, this was favorable for maintaining the low-level ascending motion. The WPSH controlled the eastern region of the South China Sea at 500 hPa, and was

located notably more eastward than that of the SC-A type events (Fig. 4b). Meanwhile, the precipitation center of the SC-C type events was mainly in Guangxi region, showing that the WPSH had little influence on the precipitation of these PHREs. Additionally, analysis of the water vapor tracks also revealed that the effect of the WPSH on SC-C type water vapor transport was not obvious. The negative OLR anomaly center reached the 90% confidence level in the Guangxi Region, indicating that the convection was stronger than the climatology, and it corresponded to strong precipitation in Guangxi. From the composite circulation at 850 hPa (Fig. 4c), the Mascarene high grew significantly stronger, and the Somali Jet stream was also stronger, than the climate mean. Correspondingly, the lower level of the South China region was controlled by southwesterly and southerly flows, which continuously transported moisture from the tropical Indian Ocean and South China Sea to the precipitation area. Consequently, sufficient water vapor for SC-C type precip-

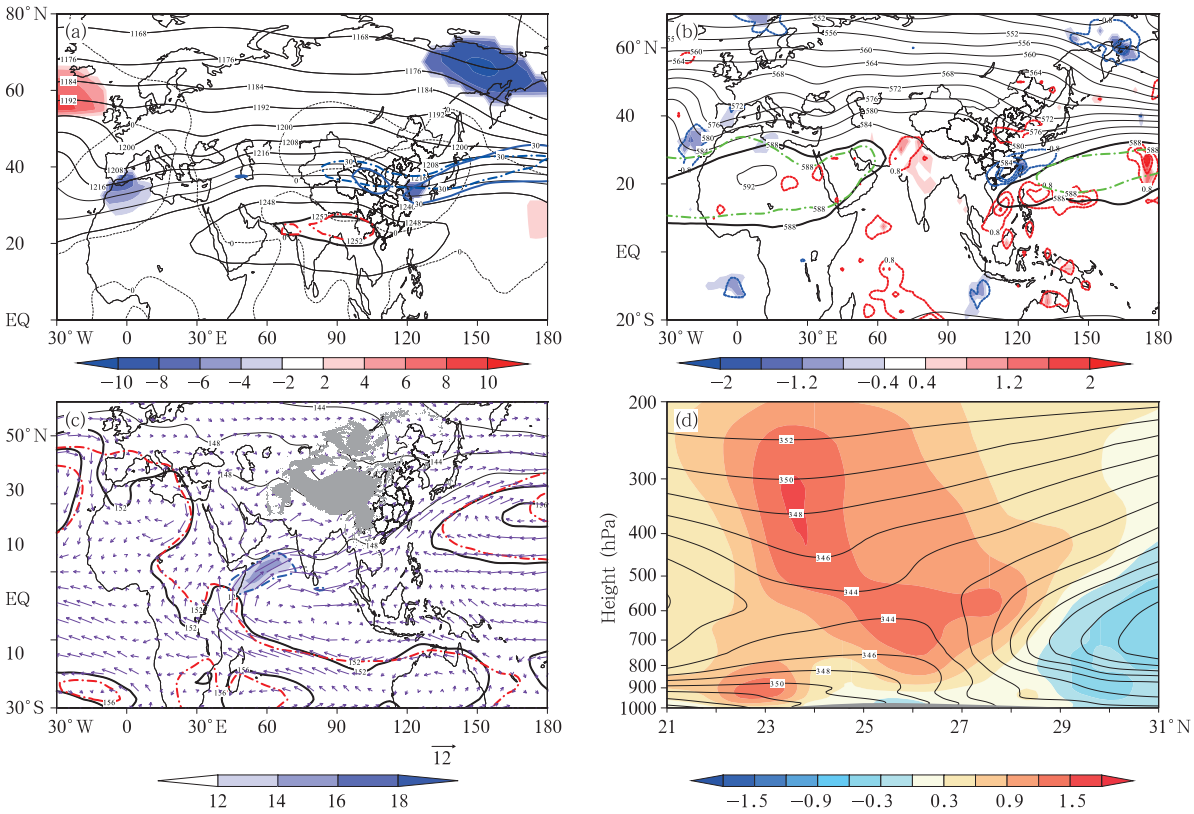

Fig. 3. Composite weather patterns for type SC-A PHREs: (a) 200-hPa geopotential height (black solid lines; dagpm; red dot-dashed lines indicate the climatic means of 1252- and 1256-dagpm isolines; black dotted lines are the zero lines of geopotential height anomaly during PHREs; shading indicates the 90% confidence level) and upper-level jet with wind speed $\geqslant$ 30 m s^{-1} (blue solid lines; the blue dot-dashed lines denote the climatic means. (b) 500-hPa geopotential height (black solid lines; dagpm; green dot-dashed lines are the climatic means of 588- and 592-dagpm isolines) and OLR anomalies (W m^{-2}; red dotted lines are positive and blue dotted lines are negative; shading indicates the 90% confidence level). (c) 850-hPa geopotential height (black solid lines; dagpm; red dot-dashed lines are the climatic means of the 152- and 156-dagpm isolines) and wind vectors (arrows; m s^{-1}; shading indicates the low-level jet; blue dot-dashed line is the climatic mean of the isoline of 12 m s^{-1}). Bold black solid lines are in (a), (b) and (c) isolines of 588 dagpm. (d) Cross-section along 114.5°E for the pseudo-equivalent temperature (black lines; K) and vertical velocity (color-shaded; $-\omega \times 10$; Pa s^{-1}) through the precipitation center (grey shading at the bottom indicates terrain). In (a–c), composite (black contours) was obtained by averaging the 8 cases based on daily data, while climatic means (various color lines) were obtained by averaging the 1980–2010 mean data over the 8 case periods.

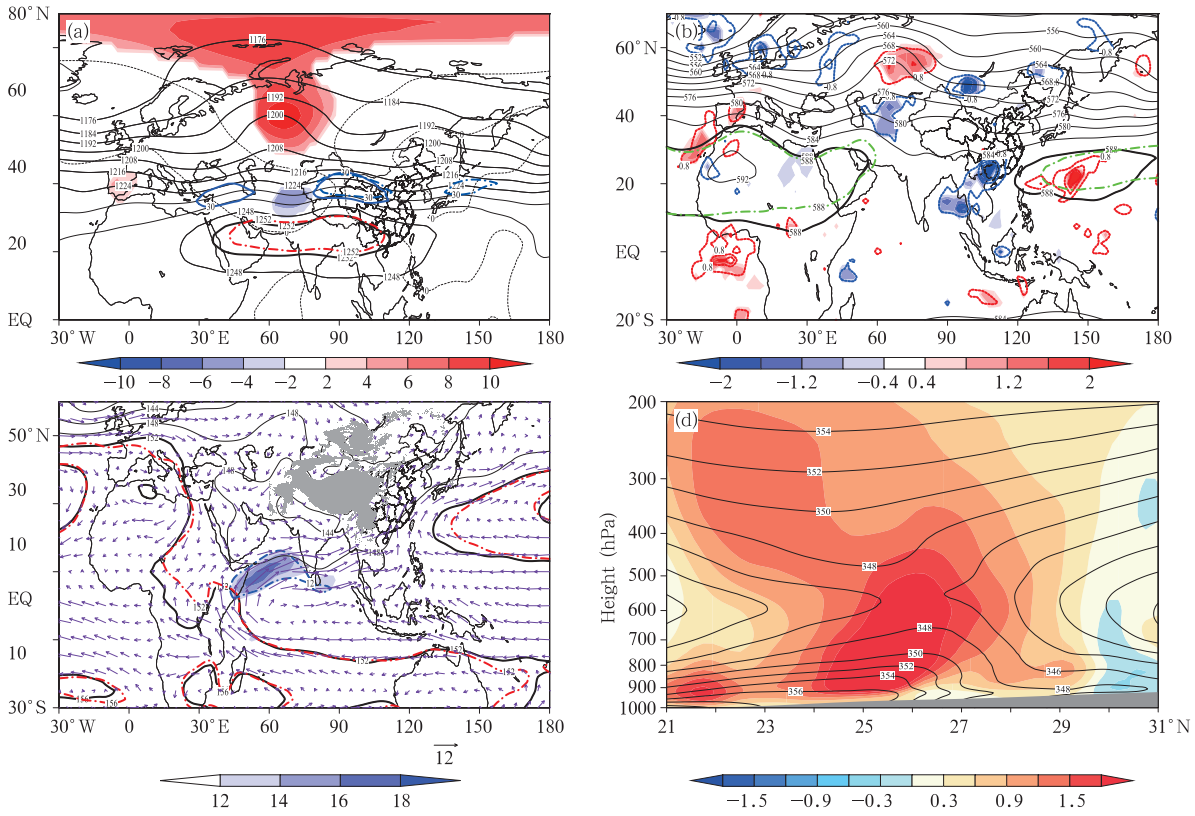

Fig. 4. (a–c) As in Figs. 3a–c, but for type SC-C PHREs. (d) As in Fig. 3d, but along 109°E for SC-C PHREs.

itation was provided via strong upward motion (Fig. 4d) over the precipitation area.

Based on the above composite analyses of the two types of PHREs, the circulation characteristics from the lower to the upper troposphere during the occurrence of these events were investigated. The main circulation characteristics of the SC-A type events can be summarized as follows. The Asian upper-level jet stream, which was located farther south, was stronger than the climatology. The mid-tropospheric trough in eastern China promoted the transport of dry-cold air to South China. Furthermore, warm and cold air gathered in the South China, triggering persistent precipitation. At the same time, water vapor was transported by the southwesterly Indian monsoon and the southwesterly wind along the northwestern edge of the WPSH, both of which provided abundant moisture for SC-A type events. For SC-C type events, the west of South China was controlled by the eastern South Asian high. The upper-level jet stream was weak and the airflow was relatively straight in the middle troposphere, which was not conducive to the southward transport of cold air. Convection in the Bay of Bengal and Guangxi Region was active; in particular, the Somali jet was significantly stronger than that associated with the SC-A type events. Additionally, the southwesterly monsoon provided adequate water vapor for the SC-C type PHREs.

4. Water vapor sources and transport for SC-A and SC-C PHREs

HYSPLIT was used to calculate the back trajectories associated with the SC-A and SC-C PHREs. According to the cluster analysis results, there were three pathways from the low latitudes for the SC-A type events (Fig. 5a); namely, from the Bay of Bengal (SC-A-CT1), the Arabian Sea (SC-A-CT2), Indonesia, and the South China Sea (SC-A-CT3). The north basically had two pathways—one that originated from the Yellow Sea (SC-A-CT4) and the other from the West Siberia Plain (SC-A-CT5). In addition to the

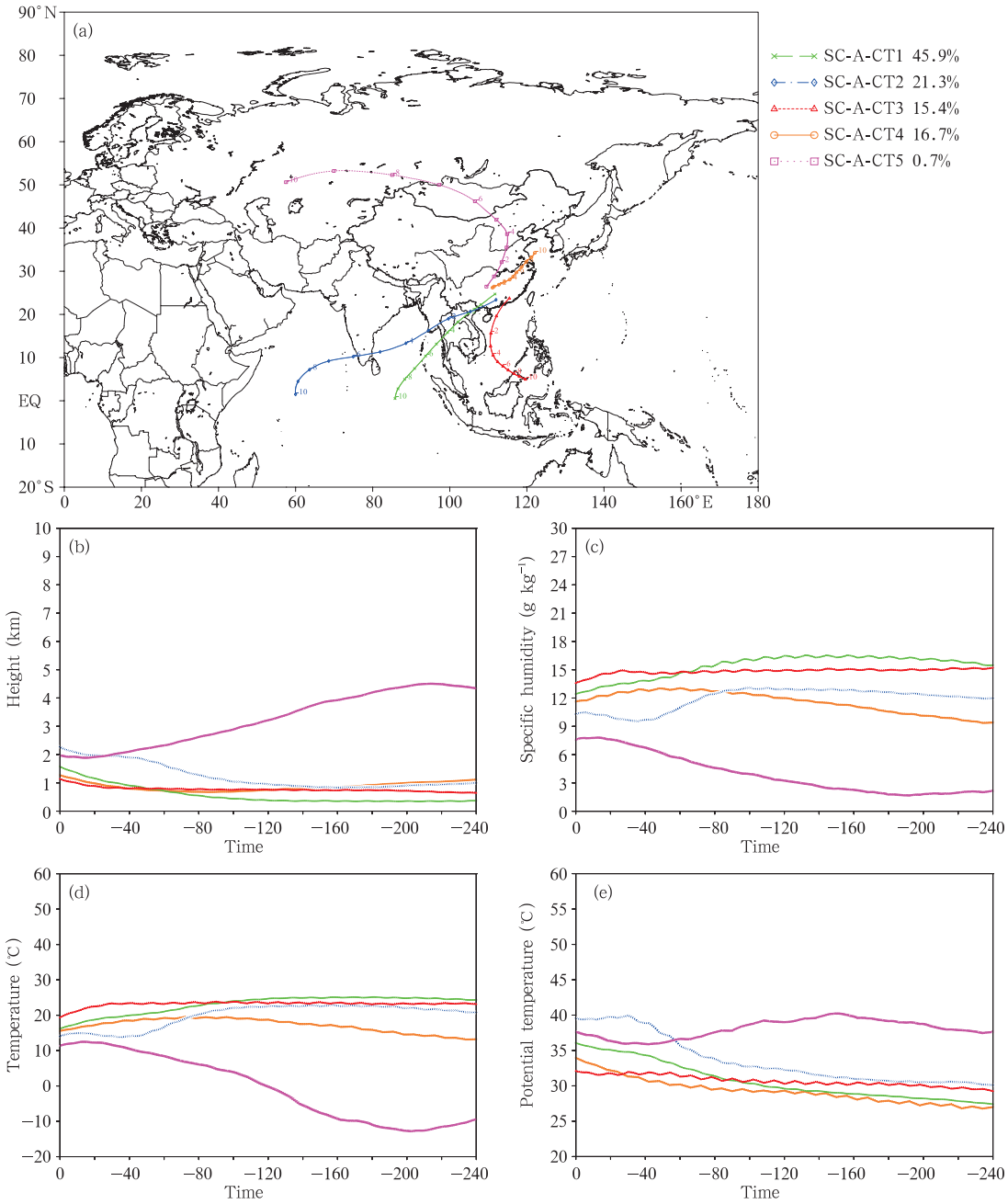

Fig. 5. Trajectory clusters of SC-A PHREs, in which the x-coordinate is the corresponding backward track with time. (a) Horizontal distribution, (b) vertical distribution, (c) specific humidity (g kg^{-1}), (d) temperature (℃), and (e) potential temperature (℃). See the first paragraph of Section 4 for definitions of different pathways indicated by the color lines.

air particles of SC-A-CT5 being from the middle troposphere (about 4000 m), other pathways were from the lower troposphere, below 2500 m (Fig. 5b). Furthermore, the moisture content and temperature of SC-A-CT5 air particles were on the low side (Figs. 5c and 5d) and the water vapor contribution rate was only 0.7%—significantly lower than the other four pathways. As a result, this pathway mainly provided dry-cold air for the SC-A PHREs. The air particles of SC-A-CT4 originating over the Yellow Sea at around 1000 m had relatively abundant moisture content and high temperature. In the process of moving south-

ward, the change in height was small and the water vapor contribution rate was 16.7%, showing that the Yellow Sea was also an important water vapor source for the SC-A type events. The SC-A-CT3 pathway had a contribution rate of 15.4%, which transported water vapor along the northwestern edge of the WPSH from the southeast to the southwest. The SC-A-CT2 pathway originated over the tropical West Indian Ocean and the source of air particles was at a height of approximately 1000 m. Furthermore, the specific humidity was able to reach up to 12 g kg^{-1}. When the air particles were traveling to Indochina, the specific humidity gradually decreased and the potential temperature increased with the increase in terrain height. As a result, water vapor condensation released latent heat due to the lifting effect of the terrain. The water vapor contribution rate of this pathway was relatively low, likely due to the decrease in East African coast cross-equatorial flow (Fig. 3c). Finally, the air parcels of the SC-A-CT1 pathway were at a height of 500 m over the Indian Ocean. Due to its low initial height over the warm water of the Indian Ocean, the moisture content of this pathway was higher than that of the SC-A-CT2 pathway, which accounted for 45.9% of the total. Because the water vapor contribution of the SC-A-CT1 and SC-A-CT2 pathways reached up to 67.2%, the tropical Indian Ocean was a major moisture source for the SC-A PHREs.

In contrast, the cluster distribution of the SC-C type events was obviously different from that of the SC-A type events (Fig. 6a). This type had no significant northern pathways, which corresponded to the weak upper-level jet stream and straight airflow at mid latitudes (Figs. 4a and 4b). This was unfavorable to the transport of cold air to South China. Aside from the two pathways that originated from the tropical Indian Ocean (SC-C-CT1) and South China Sea (SC-C-CT2), the SC-C PHREs had a lower latitude pathway (SC-C-CT3) from the western Pacific. Figure 6 illustrates the evolution of the three pathways associated with the SC-C PHREs. The initial height of these three pathways was no more than 2500 m and the moisture content was maintained within 9–15 g kg^{-1}. The SC-C-CT3 pathway that originated from the western Pacific was slightly higher than the other two pathways, with lower moisture content and constant potential temperature. The water vapor contribution rate of this pathway was only 3.8%, which was the lowest among these three pathways. However, this result did not match with the influence of the WPSH on SC-C type precipitation in the circulation analysis. The air particles of the SC-A-CT2 pathway that originated over the South China Sea below 1000 m had relatively abundant moisture content of about 12–15 g kg^{-1}. In the process of moving southward, the change in potential temperature was small and the water vapor contribution rate was 41.8%. The SC-A-CT1 pathway that originated over the tropical Indian Ocean had the largest water vapor contribution and the initial special humidity was about 14 g kg^{-1}. Furthermore, the moisture content gradually decreased due to an increase in terrain height, when air parcels arrive in Indochina. The above analysis shows that the tropical Indian Ocean and South China were two important moisture sources for the SC-C PHREs. In addition, this kind of PHRE had no significant dry-cold air, showing that southwesterly monsoon perturbations may play an important role in the triggering of precipitation at low altitude.

According to the above trajectory analysis of SC-A and SC-C PHREs, the existence of dry-cold air and differences in water vapor sources were the major discrepancies between the two PHRE types. The SC-A type events had a dry-cold air pathway that originated from the Ural Mountains and the West Siberia Plain, while the SC-C PHREs featured no obvious cold air. Moreover, the SC-A PHREs involved moist-cold air transport originating from the Yellow Sea. Although these two types of PHREs both had three pathways of water vapor transport, the tropical Indian Ocean was the largest water vapor source for the SC-A type events and the Indian Ocean and South China Sea were the largest sources for the SC-C PHREs.

5. Warm-sector rainfall characteristics of the SC-C PHREs

Based on the above analysis, the SC-C type rain-

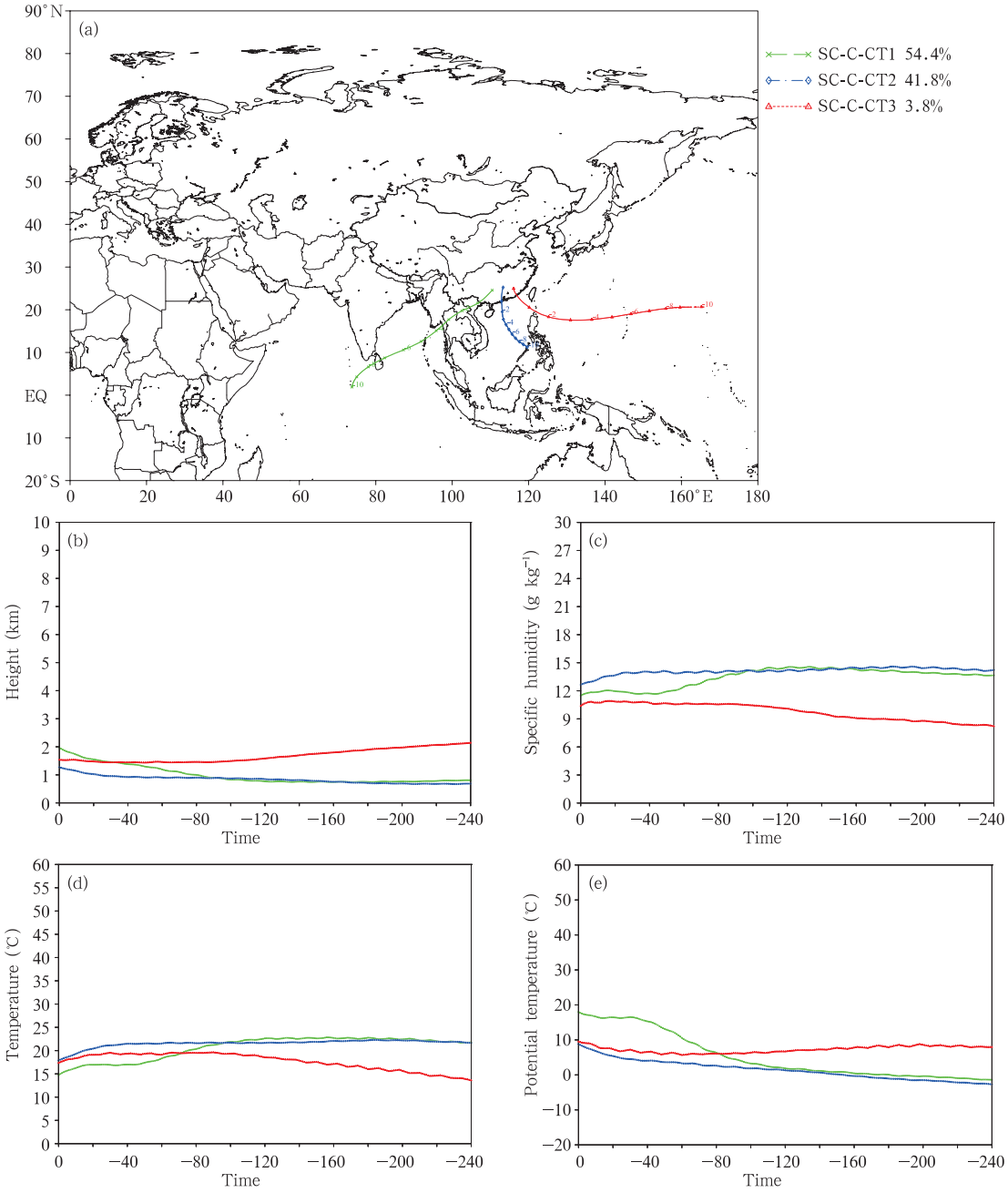

Fig. 6. As in Fig. 5, but for SC-C PHREs.

fall centers were mainly located in Guangxi Region and the dry-cold air had no significant effect on this kind of precipitation. The main reason for the precipitation may be the enhanced southwesterly monsoon perturbations, vortex activities, or convergence of southwest wind (Table 1). Such features are similar to the characteristics of warm-sector rainfall (Huang, 1986; The Editorial Committee, 2006).

In this study, the cross-section along the center of the heavy rainfall was found to be useful in summarizing the warm-sector rainfall characteristics. Besides, the potential pseudo-equivalent temperature (θ_{se}) front was obvious from surface to 850 hPa during the SC-C PHREs, with the precipitation occur-

ring ahead of the frontal zone. These features all corresponded to the warm-sector rainfall characteristics mentioned by Huang (1986). In addition, SC-C PHREs events all occurred after the onset of the South China Sea monsoon. Due to low-latitude vortex or shear line activities and strengthened monsoonal airflow over South China, the persistent rainfall events that occurred in Guangxi Region were all caused by southwesterly wind convergence. Five of the seven cases of SC-C type events were warm-sector rainfall processes caused by southwesterly wind convergence ahead of the vortex or trough (Table 1), and the other two cases were caused by wind shear. According to the low-latitude systems of influence, the SC-C PHREs could be further divided into three categories: southeast-of-the-vortex type PHREs; ahead-of-the-trough type PHREs; and wind-shear type PHREs. We analyzed three cases (27 August to 1 September 1988; 8–12 June 1991; and 16–26 June 1998) that featured high intensity precipitaion and a focused precipitaion area. We studied the time-averaged temperature advection, potential temperature, and the cross-section along the center of the heavy rainfall for the three PHREs (Fig. 7). The warm-sector rainfall that

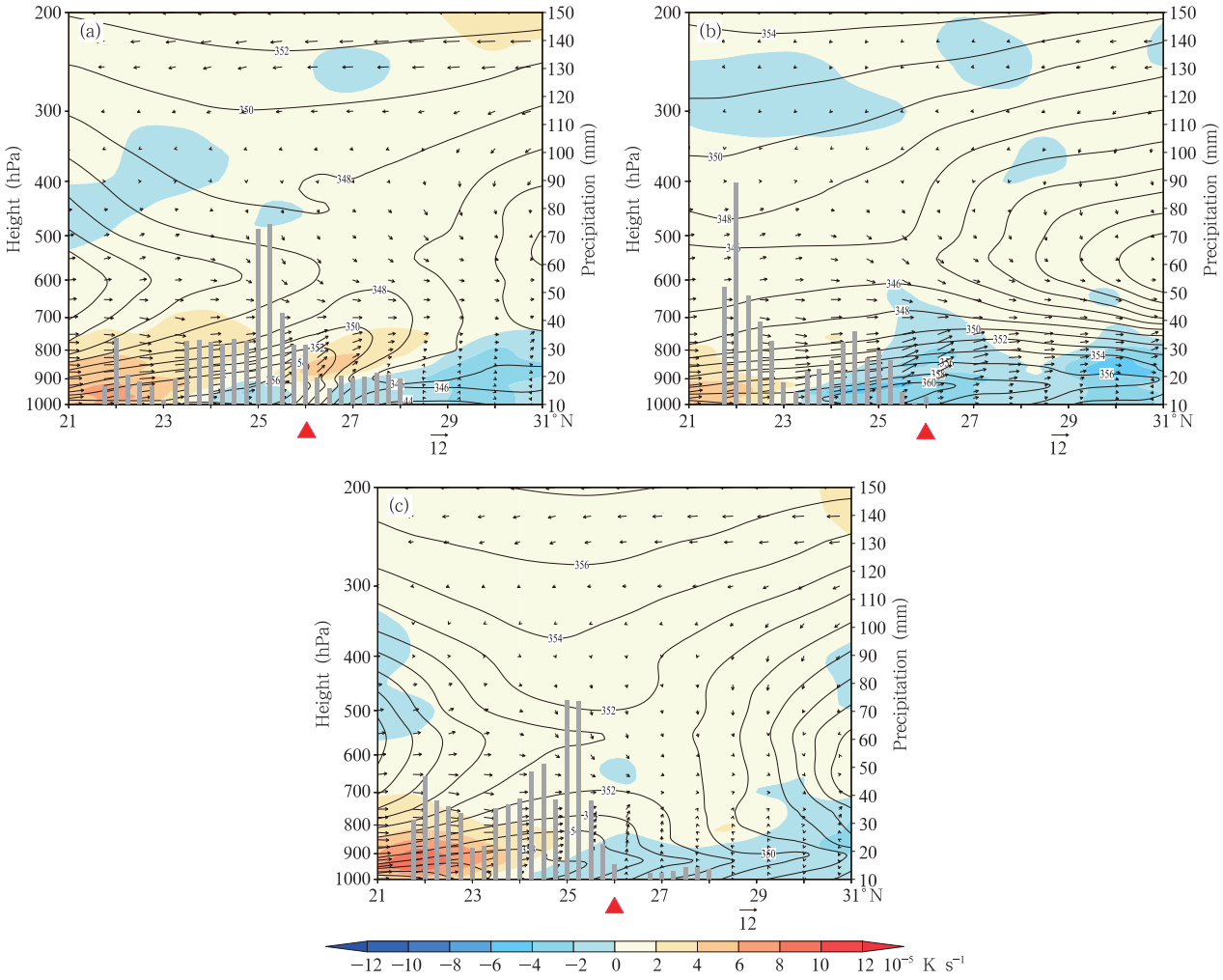

Fig. 7. Time-averaged cross-sections along the center of the heavy rainfall (109°E) for (a–c) three SC-C PHREs of potential pseudo-equivalent temperature (θ_{se}; black solid lines; K), temperature advection (color-shaded; 10^{-5} K s^{-1}), wind (vectors; m s^{-1}), and precipitation (gray bars; mm). Red triangle represents the northernmost point of the study region.

occurred from 27 August to 1 September 1988 was the southeast-of-the-vortex type. Figure 7a shows that the lower layer of the cross-section was an area of large θ_{se} values, and the middle layer was an area of low θ_{se} values. The front was to the north of 26°N and the precipitation was mainly in the warm advection area under the influence of the southerly wind from low latitudes. The second case (8–12 June 1991) was the ahead-of-the-trough type warm-sector rainfall, whose front was not obvious and was mainly influenced by southerly flow (Fig. 7b). The wind-shear type warm-sector rainfall (16–26 June 1998) presented double rain bands and the precipitation was mainly in the area south of 26°N (Fig. 7c). In addition, high θ_{se} values were mainly present in the lower layer and the precipitation was controlled by the warm-sector air. The seven SC-C PHREs all occurred in the warm-sector ahead of a front, unaffected by cold air or only for a certain period of time (figure omitted). The main circulation characteristic of SC-C type warm rainfall events was that the precipitation areas were controlled by southwesterly airflow and wind convergence. Except for the direct and/or indirect influences of the plateau troughs at high altitude, the precipitation was also influenced by small troughs and southwesterly wind convergence. In addition, the precipitation areas of the SC-C type events were mainly located in the north of Guangxi Region (Fig. 1), and the bell-mouth terrain in northeastern Guangxi had a lifting effect on the moist-warm air, which strengthened the vertical movement and favored the occurrence and maintenance of heavy rainfall (Sun and Zhao, 2002b).

6. Conclusions and discussion

Following Wang et al. (2014), an objective method was used to select regional PHREs over South China from 1981 to 2014. Based on this objective classification, the circulation characteristics, water vapor sources and transport, and the warm-sector rainfall features were investigated. The main results can be summarized as follows.

In this study, the PHREs over South China (unaffected by typhoons) included a total of 32 cases, most of which occurred in June and July of 1981–2014. Objective correlation methods were used to classify the PHREs into three types: SC-A type events, with its main rainbelt located in the coastal areas and northeast of Guangdong Province; SC-B type events, with its main rainbelt between Guangdong Province and Guangxi Region; and SC-C type events, with its main rainbelt located in the north of Guangxi Region. The SC-A type and SC-C type events were similar in frequency, which was significantly higher than that of the SC-B type events.

The circulation characteristics of the SC-A and SC-C type events can be summarized schematically in Fig. 8. For the SC-A type events (Fig. 8a), compared

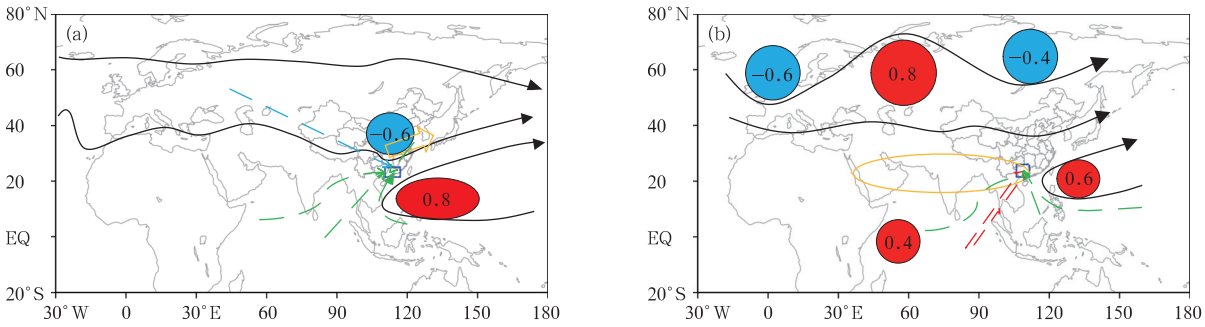

Fig. 8. Schematic representations of the circulation features for PHREs over South China: (a) type SC-A and (b) type SC-C. The small blue box represents the PHRE region; the black solid lines stand for systems at 500 hPa; the green dashed lines indicate water vapor tracks; red (blue) shading denotes positive (negative) geopotential height anomalies (numbers are the regionally averaged normalized anomaly values). In (a), the yellow arrow is the jet axis at 200 hPa; the blue dashed line denotes cold air track. In (b), the yellow solid line indicates the South Asian high; the red arrow represents the southwesterly flow.

with the climatology, the Asian upper-level jet stream was located farther south and stronger. The straight airflow at high latitudes and the troughs at midlatitudes were conducive to the delivery of dry-cold air to South China. The WPSH maintained a strong intensity and stretched westward, covering a broad region at low latitudes. This was conducive to moisture transport to the precipitation area. As for the SC-C PHREs, the jet stream at high altitude was obviously weaker than that of the SC-A type events, and the precipitation area was controlled by the eastern section of the South Asian high. In the middle troposphere, Eurasia presented a "– + –" geopotential height anomaly distribution at high latitudes, while the midlatitudes were dominated by straight airflow. Although the influence of the dry-cold air on the SC-C type events was not obvious compared with that during the SC-A type events, southwesterly monsoon perturbations and wind speed convergence in the lower troposphere played an important role in the generation and maintenance of the SC-C PHREs. Furthermore, following the enhancement of the Mascarene high, the Somali Jet strengthened the moisture transport for the SC-C type events. The SC-A type events were influenced by dry-cold air that originated from the Ural Mountains and West Siberia Plain, whereas the SC-C type events showed no obvious cold air activities. There were three water vapor pathways from low-latitude regions for the SC-A and SC-C PHREs: the tropical Indian Ocean was the main water vapor source for both types, while the Yellow Sea also provided moist-cold air for the SC-A type events, and the South China Sea for the SC-C type events.

The SC-C PHREs generally belonged to the warm-sector rainfall type. According to the systems of influence, these rainfall processes were divided into three categories: the southeast-of-the-vortex type; the ahead-of-the-trough type; and the wind-shear type. The precipitation areas of the SC-C type were mainly controlled by the southwesterly wind, which was mainly triggered by the wind speed convergence.

It is important to note that the temporal resolution of the data in this study was not high. Thus, they could only reflect the circulation characteristics in response to the occurrence of these particular events. The dataset could not be used to analyze the maintenance mechanisms and evolutionary features of PHREs. Further research is needed for this purpose, in which numerical simulations for each type of PHREs will be conducted; such work will also help to reveal differences in the weather systems among the different types of PHREs. A key finding of the present study is that the SC-C PHREs mainly belonged to the warm-sector rainfall type; however, the formation mechanism of such warm-sector rainfall is deserving of more in-depth study. Xia et al. (2006) analyzed a kind of pre-frontal warm-sector rainfall over South China and indicated that terrain had a certain effect on the lifting of moist-warm air. Therefore, the next step will be to design numerical experiments for analyzing the influence of terrain on warm-sector rainfall, in order to improve the forecasting of PHREs over South China.

REFERENCES

Bao Ming, 2007: The statistical analysis of the persistent heavy rain in the last 50 years over China and their backgrounds on the large scale circulation. *Chinese J. Atmos. Sci.*, **31**, 779–792. (in Chinese)

Chen Jiepeng, Wu Renguang, and Wen Zhiping, 2012a: Contribution of South China Sea tropical cyclones to an increase in southern China summer rainfall around 1993. *Adv. Atmos. Sci.*, **29**, 585–598.

Chen Xiangxiang, Ding Zhiying, Liu Caihong, et al., 2012b: Statistic analysis on the formation system of warm-sector heavy rainfall in May and June from 2000–2009. *J. Trop. Meteor.*, **28**, 707–718. (in Chinese)

Chen, Y., and P. M. Zhai, 2014: Two types of typical circulation pattern for persistent extreme precipitation in central–eastern China. *Quart. J. Roy. Meteor. Soc.*, **140**, 1467–1478.

Chow, K. C., H. W. Tong, and J. C. L. Chan, 2008: Water vapor sources associated with the early summer precipitation over China. *Climate Dyn.*, **30**, 497–517.

Ding, Y. H., 1992: Summer monsoon rainfall in China. *J. Meteor. Soc. Japan*, **70**, 373–369.

Draxler, R. R., and G. D. Hess, 1998: An overview of

the HYSPLIT_4 modelling system for trajectories. *Aust. Meteor. Mag.*, **47**, 295–308.

Feng, J., W. Chen, C. Y. Tam, et al., 2011: Different impacts of El Niño and El Niño Modoki on China rainfall in the decaying phases. *Int. J. Climatol.*, **31**, 2091–2101.

Fu, S. M., D. S. Li, J. H. Sun, et al., 2016: A 31-year trend of the hourly precipitation over South China and the underlying mechanisms. *Atmos. Sci. Lett.*, **17**, 216–222, doi: 10.1002/asl.645.

Fuhrmann, C. M., and C. E. Konrad II, 2013: A trajectory approach to analyzing the ingredients associated with heavy winter storms in central North Carolina. *Wea. Forecasting*, **28**, 647–667.

Hu Yamin, Du Yaodong, and Luo Xiaoling, 2013: Precipitation patterns during the "Dragon Boat Water" in South China for the recent 49 years. *Meteor. Mon.*, **39**, 1031–1041. (in Chinese)

Huang Shisong, 1986: *Rainstorms of the First Rainy Season in South China*. Scientific Press in Guangdong Province, Guangzhou, 1–7. (in Chinese)

Huang Zhong, Zhang Dong, and Lin Liangxun, 2005: Synoptic analysis of heavy rain related to monsoon trough in the latter flood season of Guangdong. *Meteor. Mon.*, **31**, 19–24. (in Chinese)

Jiang Zhihong, Liang Zhouran, Liu Zhengyu, et al., 2011: A diagnostic study of water vapor transport and budget during heavy precipitation over the Huaihe River basin in 2007. *Chinese J. Atmos. Sci.*, **35**, 361–372. (in Chinese)

Li, D. S., J. H. Sun, S. M. Fu, et al., 2016: Spatiotemporal characteristics of hourly precipitation over central eastern China during the warm season of 1982–2012. *Int. J. Climatol.*, **36**, 3148–3160.

Li, Y. F., and L. R. Leung, 2013: Potential impacts of the Arctic on interannual and interdecadal summer precipitation over China. *J. Climate*, **26**, 899–917.

Qing Tao, Shen Xinyong, Wang Weiguo, et al., 2014: Characteristics of Lagrangian transportation in a tropical deep convective process during TWP-ICE. *Chinese J. Geophys.*, **57**, 698–711.

Ren, F. M., G. X. Wu, W. J. Dong, et al., 2006: Changes in tropical cyclone precipitation over China. *Geophys. Res. Lett.*, **33**, L20702, doi: 10.1029/2006GL027951.

Santer, B. D., T. M. L. Wigley, and P. D. Jones, 1993: Correlation methods in fingerprint detection studies. *Climate Dyn.*, **8**, 265–276.

Shi Xueli and Ding Yihui, 2000: A study on extensive heavy rain processes in South China and the summer monsoon activity in 1994. *Acta Meteor. Sinica*, **58**, 666–678. (in Chinese)

Simmons, A., S. Uppala, D. Dee, et al., 2007: ERA-Interim: New ECMWF reanalysis products from 1989 onwards. *ECMWF Newsletter*, 110, ECMWF, Reading, United Kingdom, 25–35.

Sun Ying and Ding Yihui, 2002: Role of summer monsoon in anomalous precipitation patterns during 1997 flooding season. *J. Appl. Meteor. Sci.*, **13**, 277–287. (in Chinese)

Sun Jianhua and Zhao Sixiong, 2002a: A study of mesoscale convective systems and its environmental fields during the June 1994 record heavy rainfall of South China. Part I: A numerical simulation study of Meso-β convective system inducing heavy rainfall. *Chinese J. Atmos. Sci.*, **26**, 541–557. (in Chinese)

Sun Jianhua and Zhao Sixiong, 2002b: A study of mesoscale convective systems and its environmental fields during the June 1994 record heavy rainfall in South China. Part II: Effect of physical processes, initial environmental fields and topography on Meso-β convective system. *Chinese J. Atmos. Sci.*, **26**, 633–646. (in Chinese)

Sun Jianhua, Wang Huijie, Wei Jie, et al., 2016: The sources and transport of water vapor in persistent heavy rainfall events in Yangtze–Huai River valley. *Acta Meteor. Sinica,* **74**, 542–555.

Tao Shiyan, 1980: *Rainstorms in China*. Science Press, Beijing, 45–46. (in Chinese)

Tao Shiyan, Ni Yunqi, Zhao Sixiong, et al., 2001: *The Study on Formation Mechanism and Forecasting of Heavy Rainfall in the Summer 1998*. China Meteorological Press, Beijing, 183–184. (in Chinese)

Tao Shiyan, Zhang Xiaoling, and Zhang Shunli, 2004: *A Study on the Disaster of Heavy Rainfalls over the Yangtze River Basin in the Meiyu Period*. China Meteorological Press, Beijing, 1–192. (in Chinese)

The Editorial Committee, 2006: *Technical Guidance on Weather Forecasting in Guangdong Province*. China Meteorological Press, Beijing, 145–150. (in Chinese)

Tian Hong, Guo Pinwen, and Lu Weisong, 2004: Characteristics of vapor inflow corridors related to summer rainfall in China and impact factors. *J. Trop. Meteor.*, **20**, 401–408. (in Chinese)

Wang Huijie, Sun Jianhua, Wei Jie, et al., 2014: Classification of persistent heavy rainfall events over southern China during recent 30 years. *Climatic Environ. Res.*, **19**, 713–725. (in Chinese)

Xia Rudi, Zhao Sixiong, and Sun Jianhua, 2006: A study of circumstances of meso-β-scale systems of strong heavy rainfall in warm sector ahead of fronts in South China. *Chinese J. Atmos. Sci.*, **30**, 988–1008. (in Chinese)

Xie Jiongguang, Ji Zhongping, Gu Dejun, et al., 2006: The climatic background and medium-range circulation features of continuous torrential rain from April to June in Guangdong. *J. Appl. Meteor. Sci.*, **17**, 354–362. (in Chinese)

Yu, R. C., and J. Li, 2012: Hourly rainfall changes in response to surface air temperature over eastern contiguous China. *J. Climate*, **25**, 6851–6861.

Zhao Sixiong, Tao Zuyu, Sun Jianhua, et al., 2004: *Study on Mechanism of Formation and Development of Heavy Rainfalls on Meiyu Front in Yangtze River*. China Meteorological Press, Beijing, 281–282. (in Chinese)

Zhou, T. J., and R. C. Yu, 2005: Atmospheric water vapor transport associated with typical anomalous summer rainfall patterns in China. *J. Geophys. Res.*, **110**, D08104.

Zhou, T. J., R. C. Yu, H. M. Chen, et al., 2008: Summer precipitation frequency, intensity, and diurnal cycle over China: A comparison of satellite data with rain gauge observations. *J. Climate*, **21**, 3997–4010.